Analysis of Magnetic Field and Torque of Magnetic Gear with Rotor Copper Bar

Jie Li[1], Xiaocun Huang[1], and Libing Jing[2, *]

Abstract—Magnetic gear has high torque density and efficiency, and has a good application prospect in the field of low speed and high torque transmission. Accurate calculation of its air gap magnetic field is the key to analyze and design the magnetic gear. In order to improve the output torque of magnetic gear, the inner rotor is slotted, and copper bar is added in this paper. The air gap magnetic field of magnetic gear with rotor copper bar is calculated by two-dimensional analytical method. The solution domain is divided into four sub-domains, i.e., permanent magnets, air gaps, slots, and rotor copper bars. The solutions of Laplace's equation, Poisson's equation, and Helmholtz's equation are obtained by boundary conditions and continuity conditions. The distributions of air gap magnetic field, the induced current of rotor copper bars, and electromagnetic torque are obtained. The calculation results of this method are basically consistent with those of the finite element method, which proves the correctness and rationality of the analytical model.

1. INTRODUCTION

To realize the function of variable speed and torque transmission coaxial magnetic gear (CMG) changes the air gap permeance between the inner and outer layers through the middle magnetic stationary ring [1]. Compared with conventional mechanical gear, CMG has many advantages, such as no noise, no maintenance, high efficiency, high torque density, and overload protection. To improve the torque density of magnetic gear, scholars have proposed a variety of topological structures [2–4]. Especially, not only the eccentric harmonic magnetic gear structure overcomes the defects of magnetic gear due to large transmission ratio, and torque density decreases sharply, but also the torque density can reach $150 \, \text{kNm/m}^3$ [5]. The composite motor composed of coaxial magnetic gear and rotary motor has broad application prospects in low speed and high torque transmission occasions [6].

Accurate calculation of air gap magnetic field of magnetic gear is the key to analyze and design magnetic gear. Two-dimensional magnetic field can be calculated by finite element method and analytical method. The finite element method is an effective numerical analysis method, which is widely used in the field of motor design and similar magnetic field calculation. It has good accuracy in calculating the air gap magnetic field, torque, and induced eddy current with rotor copper bars [7]. The calculation accuracy of this method is high, but it takes a long time, and the size optimization is not convenient. The analytic method has clear concept, convenient adjustment of parameters, fast calculation speed, and can directly reflect the relationship between various physical quantities. Since the magnetic gear has a complex structure, including two rotating rotors and static magnetic regulating rings, the design process of finite element method is more complex and time-consuming than that of analytical method. Therefore, the analytic method is an effective method for evaluating the preliminary design of magnetic gear.

In [8], Lunbin et al. proposed a mathematical model of radial magnetized permanent magnet coaxial magnetic gear, which can accurately solve the magnetic field distribution and electromagnetic torque of magnetic gear. This method has certain guiding significance for the design of concentric magnetic gear. In [9], a similar two-dimensional analytical method was used to analyze a concentric magnetic gear with the same magnetization direction of the inner and outer rotor permanent magnets. This structure can increase the effective flux and provide additional reluctance torque. In [10], an analytical model of axial magnetic gear is established, and the air gap magnetic field and electromagnetic torque of magnetic gear are calculated by analytical method. In [11], the influences of pole number, magnetization mode, and slot size of magnetic gear on torque and unbalanced magnetic force are analyzed in detail by analytical method. In [12], the authors compared the calculation time of two-dimensional analytical method, optimized two-dimensional analytical method, and finite element method for calculating the magnetic field analysis time of magnetic gear. The results show that the analytical method and finite element method have significant differences in time.

In this paper, the magnetic field of magnetic gear with copper bar rotor is calculated by two-dimensional analytical method, and the influence of pole arc coefficient of the inner rotor on air gap magnetic field is considered. In order to improve the electromagnetic performance under overload conditions, the inner rotor increases the rotor copper bar to improve the torque. The solution field is divided into four sub-regions, namely, permanent magnet region, air gap region, slot region, and rotor copper bar region. The Laplace equation, Poisson equation, and Helmholtz equation in the corresponding region are solved by boundary conditions and continuity conditions, and the air gap magnetic field distribution can be obtained. The electromagnetic torque was calculated by the Maxwell stress tensor method. The correctness and effectiveness of the analytical model are verified by comparing the analytical results with the finite element analysis (FEA).

2. ANALYTICAL MODEL

Figure 1 shows the structural model of magnetic gear with rotor copper bar. Different from the conventional magnetic gear structure, the magnetic poles of the two permanent magnets (PMs) of the inner rotor are slotted and put into the copper bar. At the same time, the outer rotor and inner rotor are set as stationary parts, and the magnetic ring and inner rotor are rotating. The stationary ring and inner rotor are rotating and are designed as the outer rotor and inner rotor, respectively. The model consists of 7 sub-regions, namely, the inner and outer permanent magnet sub-regions (I and IV), inner and outer air gap sub-regions (II and III), slot sub-regions (i), inner rotor slot sub-regions (j), and rotor copper bar sub-regions (b). Rotor copper bar was evenly distributed in the inner rotor. Table 1 shows the parameters of magnetic gear.
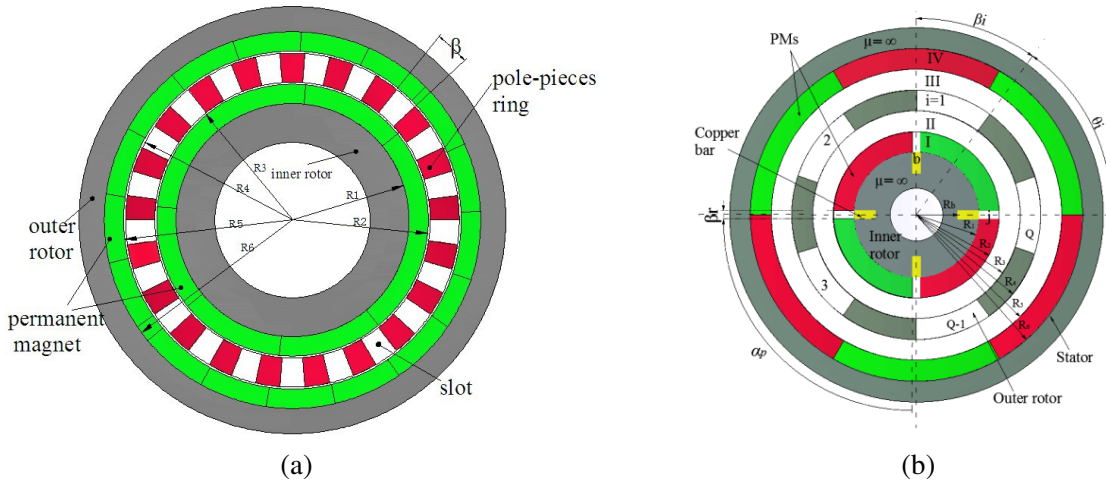

(a)   (b)

Figure 1. Magnetic gear. (a) Conventional model. (b) Magnetic gear with rotor copper bar.

Table 1. Parameters of CMG.

Symbol	Parameters	Value
R_b	Inner radius of rotor copper bar	55 mm
R_1	Outer radius of inner rotor core yoke	60 mm
R_2	Outer radius of inner rotor PM	70 mm
R_3	Inner radius of outer rotor of magnetic ring	71 mm
R_4	Outer radius of outer rotor of magnetic ring	86 mm
R_5	Inner radius of external stator PM	87 mm
R_6	Inner radius of outer stator core yoke	97 mm
p_i	Pole number of inner rotor PM	4
p_o	Pole number of outer stator PM	17
Q	Pole number of outer rotor of magnetic station ring	21
b	Copper bar of inner rotor	8
B_r	Remanence of PM	1.1 T
σ	Conductivity of copper bar	5.8×10^7 S/m
α_p	Polar arc coefficient of inner rotor	0.95
β_i	Slot width of magnetic ring	8.57°
β_r	Slot width of copper bar	2.25°

For the convenience of analysis, the following assumptions are made: (1) ignoring the end effect; (2) The permanent magnet is magnetized radially with constant permeability and remanence; (3) The permeability of the iron core is infinite; (4) The angular velocity of the rotor is known and constant; (5) The conductivity of copper bar is constant.

The magnetization of permanent magnet in two-dimensional field can be expressed as:

$$\vec{M} = M_r \, \vec{r} + M_\theta \, \vec{\theta} \tag{1}$$

Due to the radial magnetization, only the radial component M_r and tangential component M_θ are 0. The magnetization expression is r and θ function [13]:

$$M_r(\theta)\vec{r} = \sum_{n=1,3,5,\dots}^{\infty} [M_n \cos np(\theta - \theta_0)]\vec{r} \tag{2}$$

where

$$M_n = \frac{4B_r}{n\pi\mu_0} \sin\left(\frac{n\pi\alpha_p}{2}\right) \tag{3}$$

where p is the number of pole pairs of the permanent magnet, α_p the pole arc coefficient, θ_0 the offset angle between the permanent magnet and the initial reference position, and B_r the remanence of the permanent magnet.

2.1. Magnetic Field Calculation

The vector magnetic potential equations in each subregion are composed of the following equations: Laplace equation, Poisson equation, and Helmholtz equation.

In the permanent magnet regions (I and IV), the Poisson equation is:

$$\frac{\partial^2 A_{\text{I,IV}}}{\partial r^2} + \frac{1}{r}\frac{\partial A_{\text{I,IV}}}{\partial r} + \frac{1}{r^2}\frac{\partial^2 A_{\text{I,IV}}}{\partial \theta^2} = \frac{\mu_0}{r}\frac{\partial M_r}{\partial \theta} \tag{4}$$

where A_{I} and A_{IV} are the vector magnetic potential of internal and external permanent magnets, respectively; M_r is the magnetization of the permanent magnet; μ_0 is the vacuum permeability.

The Laplace equation of the inner and outer air gap regions (II and III), the slot region (i) in the magnetic regulating ring, and the inner rotor slot region (j) is:

$$\frac{\partial^2 A_{\mathrm{II},\mathrm{III},i,j}}{\partial r^2} + \frac{1}{r}\frac{\partial A_{\mathrm{II},\mathrm{III},i,j}}{\partial r} + \frac{1}{r^2}\frac{\partial^2 A_{\mathrm{II},\mathrm{III},i,j}}{\partial \theta^2} = 0 \tag{5}$$

where A_{II} and A_{III} are the vector magnetic potential in the inner and outer air gap regions, respectively; A_i and A_j are the vector magnetic potential of the outer rotor and inner rotor slot subregion, respectively.

The Helmholtz equation of rotor copper bar subregion (b) is:

$$\frac{\partial^2 A_b}{\partial r^2} + \frac{1}{r}\frac{\partial A_b}{\partial r} + \frac{1}{r^2}\frac{\partial^2 A_b}{\partial \theta^2} = j\omega_{rn}\sigma\mu_0 A_b \tag{6}$$

where A_b is the vector magnetic potential in the rotor copper bar region; ω_{rn} is the angular velocity of the nth harmonic rotating magnetic field; σ is the conductivity of copper bar.

The vector magnetic potential of each sub-region has only Z-axis component in the two-dimensional polar coordinate, so the vector magnetic potential equation (A) of each sub-region is expressed as a function of the sum of r and θ.

The expression of internal and external air gap vector magnetic potential can be expressed as [8]:

$$A_{\mathrm{II}}(r,\theta) = \sum_{n=1}^{\infty} (A_n^{\mathrm{II}} r^n + B_n^{\mathrm{II}} r^{-n})\cos(n\theta) + \sum_{n=1}^{\infty} (C_n^{\mathrm{II}} r^n + D_n^{\mathrm{II}} r^{-n})\sin(n\theta) \tag{7}$$

$$A_{\mathrm{III}}(r,\theta) = \sum_{n=1}^{\infty} (A_n^{\mathrm{III}} r^n + B_n^{\mathrm{III}} r^{-n})\cos(n\theta) + \sum_{n=1}^{\infty} (C_n^{\mathrm{III}} r^n + D_n^{\mathrm{III}} r^{-n})\sin(n\theta) \tag{8}$$

where $A_n^{\mathrm{II}}, B_n^{\mathrm{II}}, C_n^{\mathrm{II}}, D_n^{\mathrm{II}}$ and $A_n^{\mathrm{III}}, B_n^{\mathrm{III}}, C_n^{\mathrm{III}}, D_n^{\mathrm{III}}$ are constants.

For the inner permanent magnet region, the vector magnetic potential expression is:

$$A_{\mathrm{I}}(r,\theta) = \sum_{n=1}^{\infty} [A_n^{\mathrm{I}} r^n + B_n^{\mathrm{I}} r^{-n} + U_n(r)\cos(n\phi_i)]\cos(n\theta) + \sum_{n=1}^{\infty} [C_n^{\mathrm{I}} r^n + D_n^{\mathrm{I}} r^{-n} + U_n(r)\sin(n\phi_i)]\sin(n\theta) \tag{9}$$

where $A_n^{\mathrm{I}}, B_n^{\mathrm{I}}, C_n^{\mathrm{I}}, D_n^{\mathrm{I}}$ is a constant, and ϕ_i is the initial angle of the inner rotor rotation. The $U_n(r)$ in the formula can be expressed as:

$$U_n(r) = \begin{cases} 4B_r p_i r/(\pi(1-n^2)), & n = mp_i, \quad m = 1,3,5,\ldots \\ 2B_r r \ln r/\pi, & \nabla = p_i = 1 \\ 0, & elsewhere. \end{cases}$$

For the outer permanent magnet region, the vector magnetic potential expression is:

$$A_{\mathrm{IV}}(r,\theta) = \sum_{n=1}^{\infty} [A_n^{\mathrm{IV}} r^n + B_n^{\mathrm{IV}} r^{-n} + V_n(r)\cos(n\phi_o)]\cos(n\theta) + \sum_{n=1}^{\infty} [C_n^{\mathrm{IV}} r^n + D_n^{\mathrm{IV}} r^{-n} + V_n(r)\sin(n\phi_o)]\sin(n\theta) \tag{10}$$

where $A_n^{\mathrm{IV}}, B_n^{\mathrm{IV}}, C_n^{\mathrm{IV}}, D_n^{\mathrm{IV}}$ is a constant; ϕ_o is the initial angle of the outer rotor; the outer rotor is stationary. The $V_n(r)$ in the formula can be expressed as:

$$V_n(r) = \begin{cases} 4B_r p_o r/(\pi(1-n^2)), & n = mp_o, \quad m = 1,3,5,\ldots \\ 2B_r r \ln r/\pi, & \nabla = p_o = 1 \\ 0, & elsewhere. \end{cases}$$

where p_o represents the pole pairs of the permanent magnets of the outer stator.

The expressions of vector magnetic potential in the subregions of the i-slot and j-slot are as follows:

$$A_i(r,\theta) = A_0^i + B_0^i \ln r + \sum_{k=1}^{\infty} \left(A_k^i \left(\frac{r}{R_4}\right)^{\frac{k\pi}{\beta_i}} + B_k^i \left(\frac{r}{R_3}\right)^{-\frac{k\pi}{\beta_i}} \right) \cos\left[\frac{k\pi}{\beta_i}(\theta - \theta_i)\right] \tag{11}$$

$$A_j(r,\theta) = A_0^j + B_0^j \ln r + \sum_{k=1}^{\infty} \left(A_k^j (r)^{\frac{k\pi}{\beta_r}} + B_k^j (r)^{-\frac{k\pi}{\beta_r}} \right) \cos\left[\frac{k\pi}{\beta_r}(\theta - \theta_r)\right] \tag{12}$$

$A_0^i, B_0^i, A_0^j, B_0^j A_k^i, B_k^i, A_k^j, B_k^j$ are constants, and θ_i and θ_j are the position angles of the i slot of the magnetic ring and the j slot of the inner rotor, respectively. β_i and β_r are slot widths of the magnetic ring and inner rotor, respectively.

For the rotor copper bar region, the vector magnetic potential expression is:

$$A_b(r,\theta) = A_0^b J_0(\alpha r) + B_0^b Y_0(\alpha r) + \sum_{k=1}^{\infty} \left(A_k^b J_{k\pi/\beta_b}(\alpha r) + B_k^b Y_{k\pi/\beta_b}(\alpha r)\right) \cos\left[\frac{k\pi}{\beta_b}(\theta - \theta_b)\right] \qquad (13)$$

$A_0^b, B_0^b, A_k^b, B_k^b$ are constants; β_b is the slot width of rotor copper bar; θ_b is the initial position angle of rotor copper bar; J_0 and $J_{k\pi/\beta_b}$ are Bessel functions of the first kind; Y_0 and $Y_{k\pi/\beta_b}$ are Bessel functions of the second kind. In [14], the rotor copper bars are analyzed in detail.

2.2. Boundary Conditions

Figure 2 shows the boundary conditions of the rotor copper bar. Both sides and bottom of the rotor copper bar are in contact with silicon steel, and the tangential magnetic density of these boundaries is 0. Its mathematical expression is:

$$\begin{cases} A_b(R_1, \theta) = A_j(R_1, \theta) \\ \left.\dfrac{\partial A_b}{\partial r}\right|_{r=R_b} = 0 \\ \left.\dfrac{\partial A_b}{\partial \theta}\right|_{\theta=\theta_b} = 0 \\ \left.\dfrac{\partial A_b}{\partial \theta}\right|_{\theta=\theta_b+\beta_b} = 0 \end{cases} \qquad (14)$$
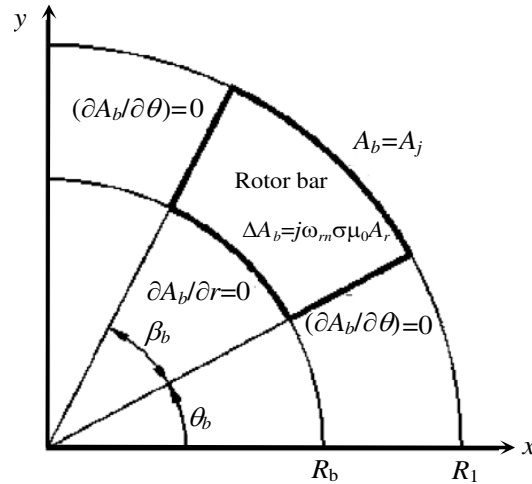

Figure 2. Boundary conditions of rotor copper bar sub-region.

Similarly, the boundary conditions of the i-slot and j-slot are shown in Fig. 3.
The i-slot boundary condition is:

$$\begin{cases} A_i(R_3, \theta) = A_{\mathrm{II}}(R_3, \theta); \quad A_i(R_4, \theta) = A_{\mathrm{III}}(R_4, \theta) \\ \left.\dfrac{\partial A_i}{\partial \theta}\right|_{\theta=\theta_i} = 0; \quad \left.\dfrac{\partial A_i}{\partial \theta}\right|_{\theta=\theta_i+\beta_i} = 0 \end{cases} \qquad (15)$$
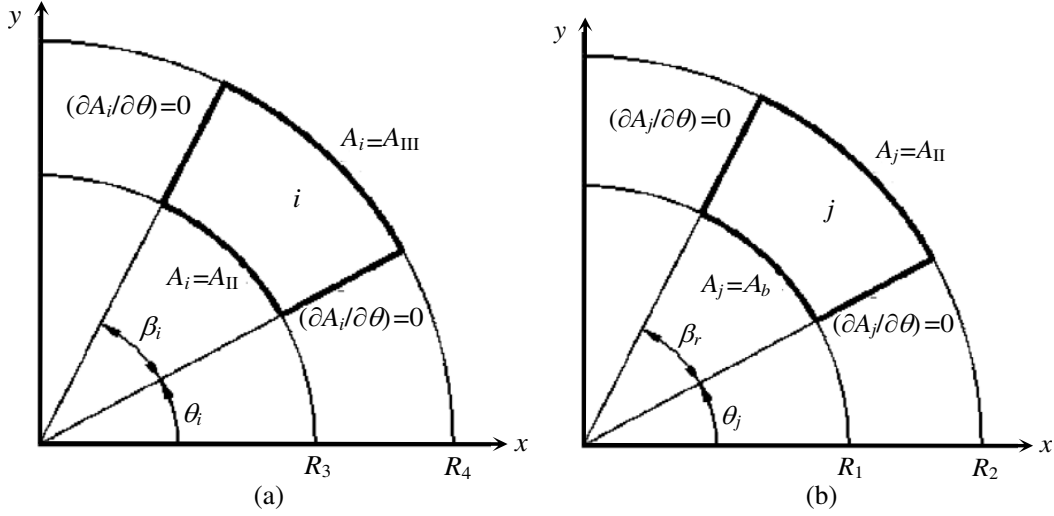
Figure 3. Boundary conditions of sub-region. (a) The i-slot boundary condition. (b) The j-slot boundary condition.

The j-slot boundary condition is:

$$\begin{cases} A_j(R_1, \theta) = A_b(R_1, \theta); \quad A_j(R_2, \theta) = A_{\mathrm{II}}(R_2, \theta) \\ \left. \dfrac{\partial A_j}{\partial \theta} \right|_{\theta=\theta_j} = 0; \quad \left. \dfrac{\partial A_j}{\partial \theta} \right|_{\theta=\theta_j+\beta_r} = 0 \end{cases} \tag{16}$$

For j-slot, the boundary continuity condition is:

$$\begin{cases} \left. \dfrac{\partial A_j}{\partial r} \right|_{r=R_1} = \left. \dfrac{\partial A_b}{\partial r} \right|_{r=R_1} \\ \left. \dfrac{\partial A_{\mathrm{II}}}{\partial r} \right|_{r=R_2} = \begin{cases} \left. \dfrac{\partial A_j}{\partial r} \right|_{r=R_2}, & \theta_j \leq \theta \leq \theta_j + \beta_r \\ 0, & \text{elsewhere.} \end{cases} \end{cases} \tag{17}$$

The radial component $(B_{\mathrm{II}r})$ and tangential component $(B_{\mathrm{II}\theta})$ of the inner air gap flux density can be obtained by derivation of the inner air gap vector magnetic potential expression according to the following formula.

$$\begin{cases} B_{\mathrm{II}r} = \dfrac{1}{r} \dfrac{\partial A_{\mathrm{II}}}{\partial \theta} \\ B_{\mathrm{II}\theta} = -\dfrac{\partial A_{\mathrm{II}}}{\partial r} \end{cases} \tag{18}$$

Therefore, the radial component and tangential component of the inner air gap flux density are respectively expressed as:

$$B_{\mathrm{II}r}(r, \theta) = \sum_{n=1}^{\infty} -(A_n^{\mathrm{II}} n r^{n-1} + B_n^{\mathrm{II}} n r^{-n-1}) \sin(n\theta) + \sum_{n=1}^{\infty} (C_n^{\mathrm{II}} n r^{n-1} + D_n^{\mathrm{II}} n r^{-n-1}) \cos(n\theta) \tag{19}$$

$$B_{\mathrm{II}\theta}(r, \theta) = \sum_{n=1}^{\infty} -(A_n^{\mathrm{II}} n r^{n-1} - B_n^{\mathrm{II}} n r^{-n-1}) \cos(n\theta) + \sum_{n=1}^{\infty} -(C_n^{\mathrm{II}} n r^{n-1} - D_n^{\mathrm{II}} n r^{-n-1}) \sin(n\theta) \tag{20}$$

Similarly, the radial and tangential components of the outer air gap flux density can also be obtained and are no longer listed here.

2.3. Current Density and Current of Rotor Copper Bar

According to the current density equation, the expression of induced current density in rotor copper bar is

$$J_b(r, \theta) = -j\omega_{rn}\sigma A_b(r, \theta) \tag{21}$$

Therefore, the induced current in the b-th rotor copper bar is:

$$I_b = \int_{R_b}^{R_1} \int_{\theta_b}^{\theta_b+\beta_b} J_b(r, \theta) r dr d\theta \tag{22}$$

Substituting Eq. (21) into Eq. (22), the current expression of each rotor copper bar can be obtained:

$$I_b = \frac{-j\omega_{rn}\sigma A_0^b \beta_b R_1}{\alpha} \times \left(\frac{J_1(\alpha R_b)Y_1(\alpha R_1) - J_1(\alpha R_1)Y_1(\alpha R_b)}{J_0(\alpha R_b)Y_1(\alpha R_1) - J_1(\alpha R_1)Y_0(\alpha R_b)} \right) \tag{23}$$

In the formula, $\alpha_2 = -j\sigma\omega_{rn}\mu_0$, J and Y are the first Bessel function and the second Bessel function, respectively.

3. ELECTROMAGNETIC TORQUE

Electromagnetic torque is one of the important parameters to measure the performance of the magnetic gear. According to the Maxwell stress tensor method, the radial and tangential components of inner air gap flux density calculated by formula (19) and formula (20) are substituted into formula (14). The electromagnetic torque of the inner rotor of magnetic gear is obtained as follows:

$$T_{em} = \frac{L_{ef}}{u_0} \int_0^{2\pi} r^2 B_{\mathrm{II}r} B_{\mathrm{II}\theta} d\theta \tag{24}$$

where L_{ef} is the axial effective length of magnetic gear; r is any circumference radius in the inner air gap. Similarly, the electromagnetic torque output by the magnetic regulating ring can also be obtained.

4. CALCULATION EXAMPLES AND COMPARISON

In order to verify the accuracy and effectiveness of the analytical model, this paper uses Matlab to program the analytical expression of each field and compares the analytical calculation results with the FEA results under Ansys software. The selected model parameters are shown in Table 1. In the analytical model, the harmonic number of the magnetic field in the air gap region is 150, and the harmonic number of the magnetic field in the slot region is 50.

The initial phase angles of the outer stator permanent magnet and the magnetic regulating stator slot are set to 0°, and the rotation speed of the inner rotor is set to 525 r/min. At a certain time, the magnetic line of the magnetic gear and the eddy current distribution of the rotor copper bar are shown in Fig. 4.

Figure 5 shows the comparison between the analytical calculation results of radial magnetic density and tangential magnetic density at the middle of the air gap in the inner layer of the magnetic gear ($r = 70.5$ mm) and the FEA results.

Figure 6 shows the comparison between the analytical calculation results of radial magnetic density and tangential magnetic density at the middle of the outer air gap of the magnetic gear ($r = 86.5$ mm) and the FEA results.

It can be seen from Fig. 5 and Fig. 6 that the radial and tangential air-gap magnetic densities of the inner and outer layers of the magnetic gear with rotor copper bars calculated by the analytical method are basically consistent with those calculated by the FEA in the waveform, which verifies that the analytical model proposed in this paper is accurate and effective.

Figure 7 shows the current density distribution of a rotor copper bar from the bottom of the rotor slot to the top of the slot.

It can be seen from Fig. 7 that due to the skin effect, the current density of the rotor copper bar near the slot is large. The current density at the end of the rotor copper bar at the bottom of the slot is small. The results obtained by the analytical method are in good agreement with the FEA results.
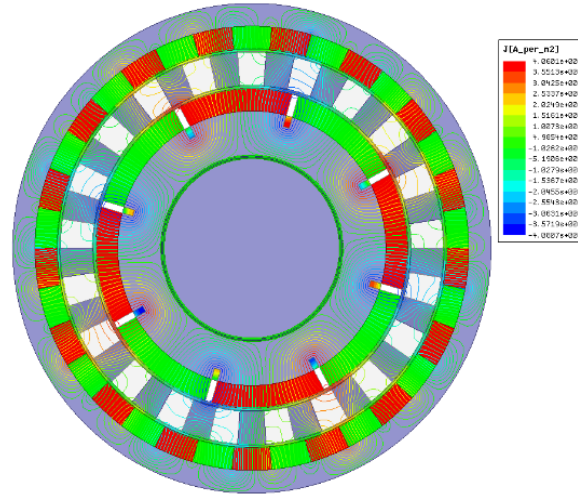
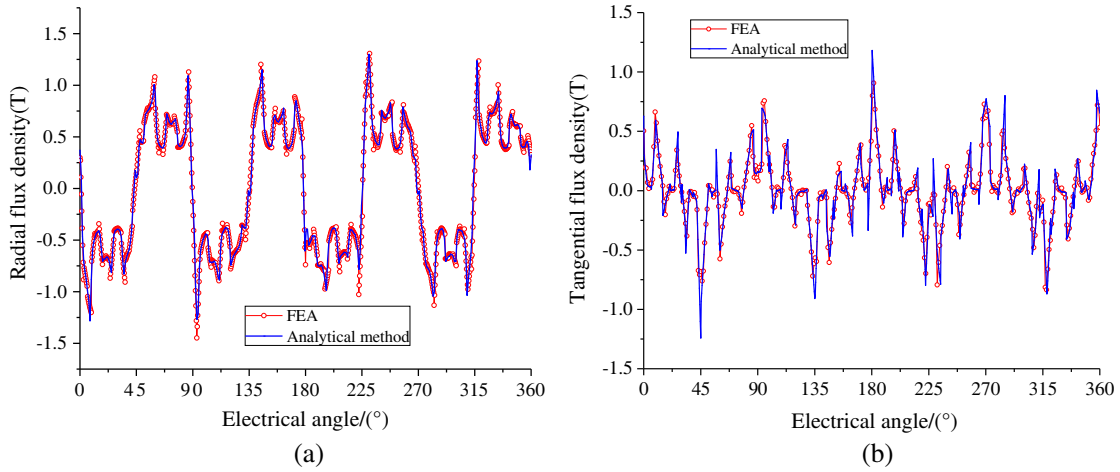**Figure 4.** Distribution of magnetic line and eddy current of copper bar.

Figure 5. Flux density distribution in the inner air gap: (a) Radial component; (b) Tangential component.
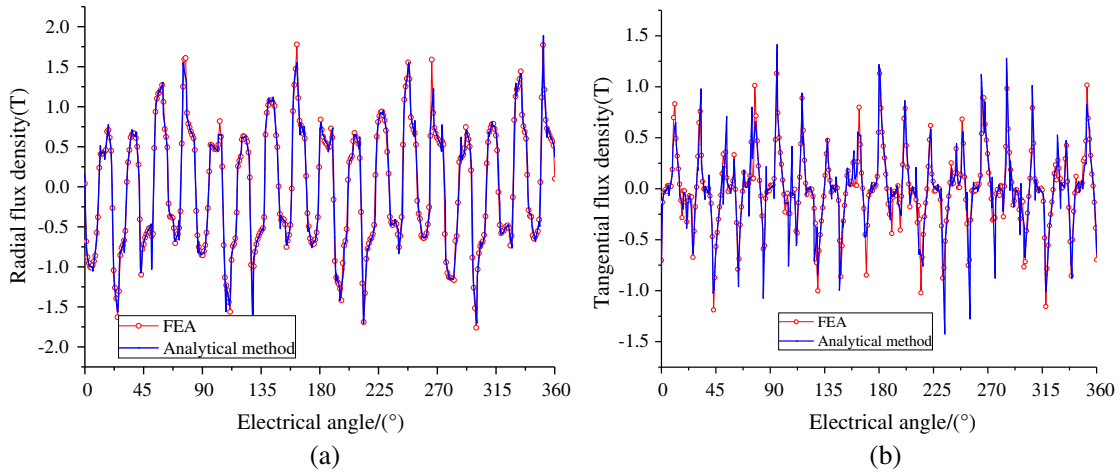

Figure 6. Flux density distribution in the outer air gap: (a) Radial component; (b) Tangential component.
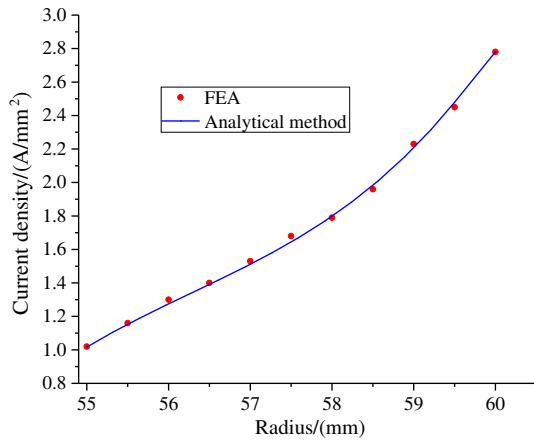
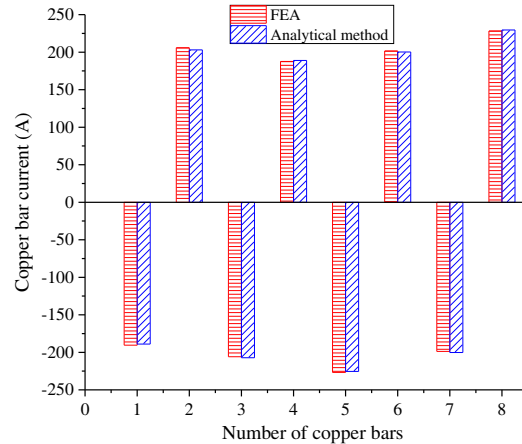**Figure 7.** Current density distribution.

Figure 8. Current distribution of rotor copper bar.

According to formula (23), the total current of each rotor copper bar can be calculated. The results of analytical method and FEA are shown in Fig. 8. It can be seen from the figure that the analytical calculation results of rotor copper bar current are basically consistent with the FEA results.

Figure 9 shows the static torque comparison diagram of the magnetic gear. The position of the magnetic regulating rotor and outer stator is fixed. The high-speed inner rotor is rotated from 0° to 45°, and a point is taken every 1°. The analytical solution of the static torque of the magnetic gear can be calculated by Equation (24). At the same time, the analytical results are compared with the FEA results.
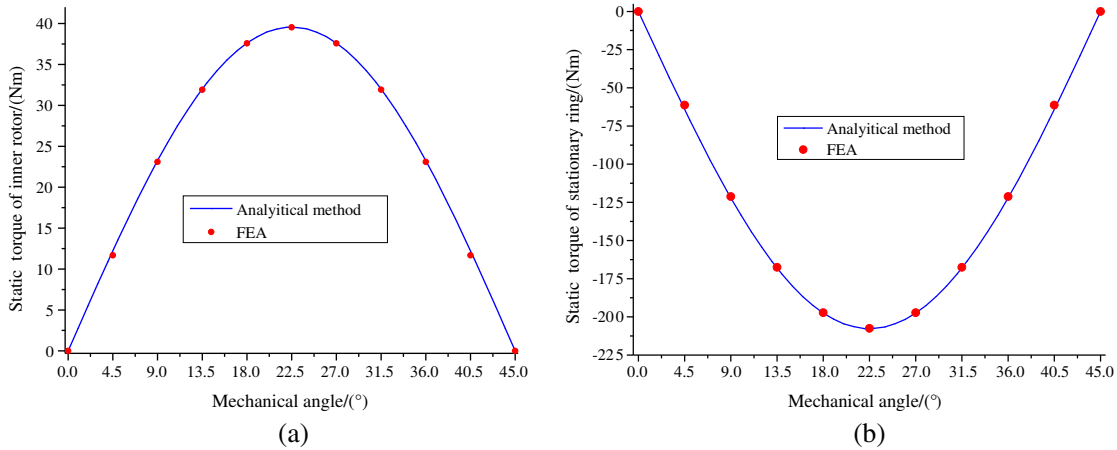

**Figure 9.** Static torque: (a) Inner rotor; (b) Outer rotor.

It can be seen from Fig. 9 that the static torque of the inner rotor and the rotor of the magnetic ring calculated by the analytical method is sine wave. The analytical calculation results are consistent with the finite element calculation results. The ratio of the torque value at the same position is 5.25 : 1, which is in line with the magnetic gear transmission ratio. When the inner rotor rotates to 22.5°, the two torque values reach the maximum.

Figure 10 is the steady-state torque analytical calculation results of two rotors output at a certain rotating speed. It can be seen from the figure that the ratio of the output torque value of the inner rotor and the magnetic regulating ring is 5.25 : 1. Compared with the conventional coaxial radial magnetization magnetic gear, the torque output value increased from 178.04 Nm to 207.66 Nm. The main reason is the magnetoresistance effect of copper bar eddy current in rotating magnetic field.

Table 2. Time comparison.

Type	Analytical method	FEA
Time(s)	2.39	48.67

Table 2 shows the time consumed by the two calculation methods. It can be seen that the analytical method has the advantage of calculation time.
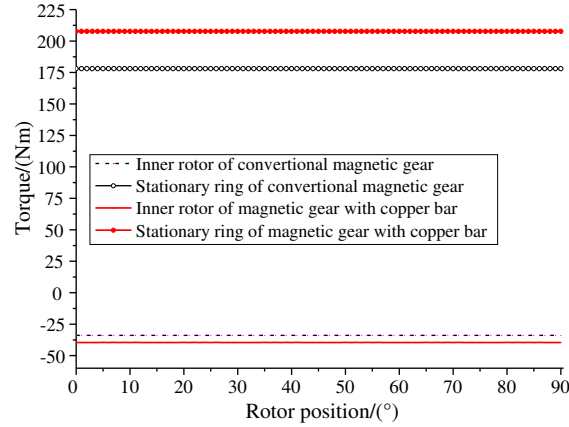
Figure 10. Electromagnetic torque.

5. CONCLUSION

The magnetic field distribution and electromagnetic torque of magnetic gear with copper bar in inner rotor are calculated by subdomain model analysis method. The analytical model of magnetic gear with rotor copper bar is established, and the Laplace equation, Poisson equation, and Helmholtz equation of various subregions are connected by boundary conditions and boundary continuity conditions to obtain the vector magnetic potential equation of each region. The air gap flux density and electromagnetic torque of the inner and outer layers of the magnetic gear are calculated by a numerical example model. The analytical results are in good agreement with the finite element calculation results, which verifies the correctness and effectiveness of the analytical method. At the same time, the output torque increases due to the existence of rotor copper bar eddy current, which can improve the carrying capacity of magnetic gear. Therefore, the proposed analytical model can provide a reference for the optimal design of magnetic gear.

REFERENCES

1. Atallah, K. and D. Howe, "A novel high-performance magnetic gear," *IEEE Trans. Magn.*, Vol. 37, No. 4, 2844–2846, Jul. 2001
2. Jing, L., Z. Huang, J. Chen, and R. Qu, "An asymmetric pole coaxial magnetic gear with unequal Halbach arrays and spoke structure," *IEEE Trans. Appl. Supercond.*, Vol. 30, No. 4, 1–5, Art No. 5200305, Jun. 2020.
3. Zhang, X., X. Liu, and Z. Chen, "A novel dual-flux-modulator coaxial magnetic gear for high torque capability," *IEEE Trans. Energy Conversion*, Vol. 33, No. 2, 682–691, Jun. 2018.
4. Jing, L., Z. Huang, J. Chen, and R. Qu, "Design, analysis, and realization of a hybrid-excited magnetic gear during overload," *IEEE Trans. Ind. Appl.*, Vol. 56, No. 5, 4812–4819, Sept.– Oct. 2020.

5. Rens, J., K. Atallah, S. Calverley, and D. Howe, "A novel magnetic harmonic gear," *2007 IEEE International Electric Machines & Drives Conference*, 698–703, 2007.

6. Zhao, X. and S. Niu, "Design and optimization of a new magnetic-geared pole-changing hybrid excitation machine," *IEEE Trans. Indus. Electr.*, Vol. 64, No. 12, 9943–9952, Dec. 2017.

7. Khang, H. and A. Arkkio, "Eddy-current loss modeling for a form-wound induction motor using circuit model," *IEEE Trans. Magn.*, Vol. 48, No. 2, 1059–1062, Feb. 2012.

8. Lubin, T., S. Mezani, and A. Rezzoug, "Exact analytical method for magnetic field computation in the air gap of cylindrical electrical machines considering slotting effects," *IEEE Trans. Magn.*, Vol. 46, No. 4, 1092–1099, Apr. 2010.

9. Aiso, K., K. Akatsu, and Y. Aoyama, "A novel reluctance magnetic gear for high-speed motor," *IEEE Trans. Ind. Appl.*, Vol. 55, No. 3, 2690–2699, May/Jun. 2019.

10. Lubin, T., S. Mezani, and A. Rezzoug, "Development of a 2-D analytical model for the electromagnetic computation of axial-field magnetic gears," *IEEE Trans. Magn.*, Vol. 49, No. 11, 5507–5521, Nov. 2013.

11. Rahideh, A., A. Vahaj, and M. Mardaneh, "Two dimensional analytical investigation of the parameters and the effects of magnetization patterns on the performance of coaxial magnetic gears," *Electrical Systems Trans.*, Vol. 7, No. 3, 230–245, May 2017.

12. Desvaux, M., B. Traullé, R. Le Goff Latimier, S. Sire, B. Multon, and H. Ben Ahmed, "Computation time analysis of the magnetic gear analytical model," *IEEE Trans. Magn.*, Vol. 53, No. 5, 1–9, May 2017.

13. Zhu, Z. and D. Howe, "Instantaneous magnetic field distribution in brushless permanent magnet DC motors. II. Armature-reaction field," *IEEE Trans. Magn.*, Vol. 29, No. 1, 136–142, Jan. 1993.

14. Lubin, T., S. Mezani, and A. Rezzoug, "Analytic calculation of eddy currents in the slots of electrical machines: Application to cage rotor induction motors," *IEEE Trans. Magn.*, Vol. 47, No. 11, 4650–4659, Nov. 2011.